Measurement of Impurity Transport Coefficients in the Confined Plasma of ASDEX Upgrade

R. Dux, A. G. Peeters, A. Gude, A. Kallenbach, R. Neu and the ASDEX Upgrade team
Max-Planck-Institut für Plasmaphysik, EURATOM Association, Garching, Germany
e-mail: Ralph.Dux@ipp.mpg.de

Abstract: For ASDEX Upgrade H-Mode discharges, the core plasma impurity transport has been investigated in the quiet phase between sawtooth crashes. For the elements Ne, Ar, Kr and Xe the diffusion coefficient in the center is $D \leq 6 \times 10^{-2}\mathrm{m}^2/\mathrm{s}$ and rises with the radial distance from the center. With increasing Z number the transport becomes strongly convective with inwardly directed drift velocities that produce very peaked impurity densities for high Z. The calculated neoclassical diffusion coefficient and drift velocity are close to the experimental values for the lower Z elements Ne and Ar. The calculated drift velocity is too small by a factor of 10 for Kr and Xe. For these elements, toroidal rotation of the plasma leads to an increased impurity density on the outboard side of the flux surfaces which is not taken into account by the neoclassical calculations. The outboard/inboard ratio for Kr is ≈ 1.5 and the toroidal Mach number $M_{tor} \approx 2$.
Investigations of Si and Ne transport in the edge region, i.e. the region of the temperature pedestal and the steep temperature gradient zone, yield an inwardly directed drift velocity in the quiet phase between ELMs. The inward pinch is observed in the radial range of the steep temperature gradient. The transport induced by an ELM is best described by a very high radial diffusion coefficient rather than by an outwardly directed drift velocity.

1. Introduction

It has been found on several tokamaks that the radial impurity transport in the confined plasma strongly decreases from the edge to the core [1,2]. Furthermore, the transport coefficients are temporally modulated due to macroscopic instabilities, i.e. in the core due to sawteeth and at the edge of H-mode plasmas due to ELMs. In ASDEX Upgrade H-mode discharges measurements of impurity transport with high temporal resolution have been performed to determine the transport coefficients in the time intervals between such macroscopic instabilities.

2. Impurity Transport in the Core

Four different gases (Ne, Ar, Kr, and Xe) were puffed at the mid-plane during the steady-state phase of type-I ELMy H-mode discharges with neutral beam heating power P_{NI}=5 MW, toroidal field B_T=2.5 T, plasma current I_p=1 MA and safety factor q_{95}=4. The line averaged density was $\bar{n}_e$=7.5$\times 10^{19}\mathrm{m}^{-3}$ which is 60% of the Greenwald limit $\bar{n}_{GW}$. Three soft X-ray (SXR) cameras with 100µm thick Be-filters (detection efficiency >0.5 for photons in the energy range 2.5-15 keV) served as the main diagnostic tool for this study. Using time averaged data with a time resolution of $\Delta t_{\mathrm{av}} \approx 1$ ms, the soft X-ray radiation fluxes from typically 65 lines-of-sight were unfolded assuming an emissivity profile that is constant on flux surfaces. This one dimensional emissivity profile $\varepsilon_{sxr}(\rho)$ represented all measured radiation fluxes with deviations below 5% (ρ denotes the poloidal flux label). To reduce the background, the emissivity modulation, which was observed during a time interval Δt=150 ms before the gas injection, was assumed to persist during the puff phase. Thus, the change $\Delta\varepsilon_{sxr}$ due to the puffed impurity was obtained by subtracting a time dependent background. An example for this procedure is given in Fig. 1.

From $\Delta\varepsilon(\rho)$ the impurity density profiles $n_I(\rho)$ of the puffed impurity were calculated using measured electron density and temperature profiles. The radiative power coefficient L_I^{sxr} of the respective impurity folded with the energy dependence of the detection efficiency of the SXR detectors (including the Be foil) was derived from a collisional-radiative model (ADAS database [3]). For $t - t_{crash} \geq 3$ms the fractional abundances are nearly in ionisation equilibrium and are

only a function of n_e and T_e [2]. It should be noted that for the transport analysis the absolute value of L_I^{sxr} is not important, mainly the temperature dependence, which is rather flat in the respective T_e interval, governs the resulting shape of the impurity profiles.

For the extraction of the diffusion coefficient D and the drift velocity v, the radial transport equation was solved for a time interval from 3ms after the last sawtooth crash to 3ms before the next crash in the radial range $\rho<0.4$. The initial distribution at $t_{crash}+3$ms and the density development at $\rho=0.4$ were chosen as the boundary conditions for the solution. A constant value was used for D and a linear function for the drift parameter $\alpha = \mathrm{v}a^2/(2Dr)$. The three coefficients of these test functions were computed by applying a non-linear χ^2–fit to the measured density development for $\rho<0.4$.

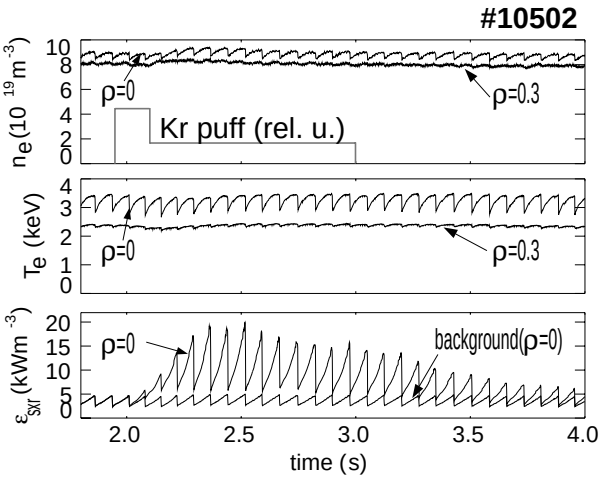

FIG. 1: For t=1.95-3.0s Kr was puffed into the discharge. The electron density n_e and electron temperature T_e in the center and at ρ=0.3 ($q\approx1$) are weakly disturbed. In the third frame the time traces of the central soft X-ray emissivity ε_{sxr} and the background emissivity are depicted.

An example of the fitting procedure is shown in Fig. 2 where one sawtooth period for Kr is depicted. Note, that the sawtooth period is too short to reach an equilibrium distribution of the impurity density and that the sawtooth crash leads to a flattening of the Kr density profile. Assuming a standard deviation of 20% for the impurity density the standard deviation of D and v was calculated from the curvature of χ^2 in the fit parameter space and is shown as bands in Fig. 2a.

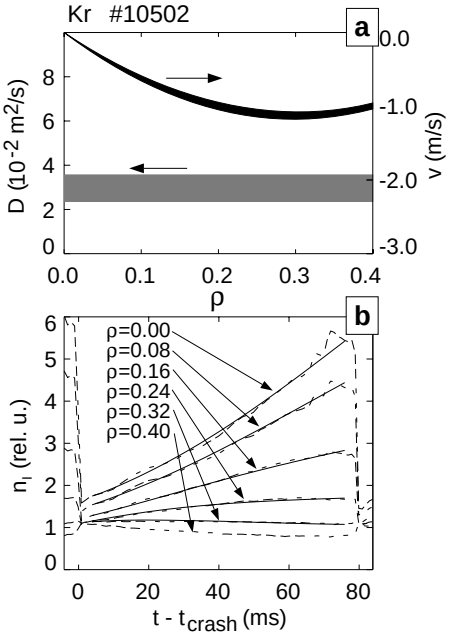

FIG. 2: Kr density evolution for several poloidal flux labels ρ (Fig. 2b, dashed lines) and the solution of the transport equation (Fig. 2b, solid lines) with D and v from Fig. 2a.

Fig. 3 shows the line averaged diffusion coefficient $\langle D\rangle$ and drift velocity $\langle \mathrm{v}\rangle$ for the radial range $0.1<\rho<0.3$ obtained from typically 10 sawtooth cycles versus the line averaged impurity charge $\langle Z\rangle$ in the same radial range. Negative values of $\langle \mathrm{v}\rangle$ represent inwardly directed drift velocities and positive values outwardly directed drift velocities. With rising impurity charge Z the convective transport increasingly dominates over the diffusive transport which is very small with $\langle D\rangle \leq 6\times10^{-2}\mathrm{m}^2/\mathrm{s}$. The drift velocity is always inwardly directed. For Kr and Xe the ratio $\langle \mathrm{v}/D\rangle$ reaches enormous values of $\langle \mathrm{v}/D\rangle \approx -35\mathrm{m}^{-1}$.

Neoclassical transport parameters were calculated with STRAHL/NEOART. STRAHL solves the coupled set of radial transport equations for every ion stage [2,4]. NEOART solves for a given impurity charge state distribution the set of linear coupled equations for the parallel velocities [5]. The resulting neoclassical transport parameters are the sum

of a classical, a Pfirsch-Schlüter and a banana-plateau term [6]. The classical fluxes are given by Eq.(5.9) and (5.10) in Section 5 of Hirshman and Sigmar [6]. The equations for the banana plateau contribution are equal to that used by Houlberg [7]. The Pfirsch-Schlüter contribution is calculated from the coupled equations (6.1-2) and (6.14-15) of Hirshman and Sigmar [6], as described in Ref. [8]. NEOART includes the collisions of the considered impurity with the main plasma ions and all other impurities. Toroidal rotation of the plasma is not taken into account. Equal temperatures of main ion D and impurities $T_D = T_I = T$ was assumed.

The neoclassical values are shown in Fig. 3 as bands representing the three cases with and without inclusion of collisions with C/O for a flat and a peaked concentration profile with $c_C \approx 1\%$ and $c_O \approx 0.1\%$. The total neoclassical diffusion coefficient is dominated by the banana-plateau values for low Z and by the sum of the classical and the Pfirsch-Schlüter contributions for high Z. The diffusion coefficient D_{neo} decreases with rising Z and is in the same range as the measurements. Anomalous diffusion is obviously ineffective in the plasma center. The drift velocity v_{neo} is dominated by the banana-plateau value for all Z and is more or less constant. For low to medium Z the measurement is well reflected by v_{neo}, for high Z the deviation is strong. The neoclassical calculations assume constant impurity density on a flux surface and the poloidal variation of the impurity density due to toroidal rotation of the plasma is small for the lighter elements Ne and Ar. However, for the heavier elements Kr and Xe with Mach numbers around 2, poloidal asymmetries are important. For Kr, the asymmetry is clearly observable and the density on the outboard side exceeds the inboard value by up to 50%. This effect is not taken into account by the neoclassical calculations and might account for the discrepancy of the transport coefficients.

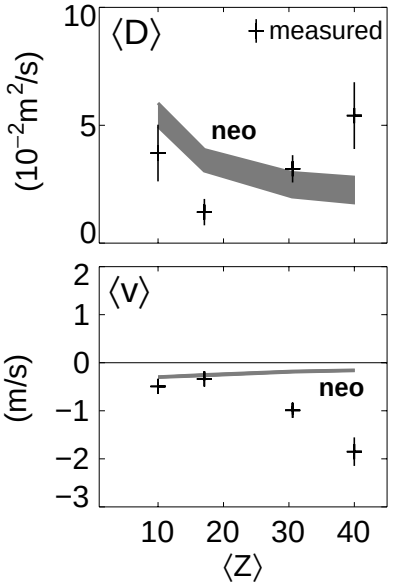

FIG. 3: Line averaged values over the radial range 0.1<ρ<0.3 of measured and neoclassical diffusion coefficient D and drift velocity v *as a function of the mean atomic charge of the impurity* $\langle Z \rangle$ *in that radial range. The neoclassical values are shown as bands representing the cases without and with collisions with C/O.*

The good agreement of measured and neoclassical transport coefficients for the elements with lower Z creates a basis to predict core impurity transport in scenarios without sawteeth ('advanced' tokamak) or with infrequent sawtooth oscillations (ignited tokamak plasma) [5].

3. Impurity Transport in the Edge

The transport of Si and Ne in the edge region of H-mode plasmas was investigated. For H-Mode discharges with type-I ELMs and ELM frequency $f_{ELM} \approx 100$Hz, a slow radial shift of the plasma column by ΔR=3.5 cm was performed during the plateau phase of the discharge. The discharges had neutral beam heating power P_{NI}=5 MW ($D \rightarrow D^+$), toroidal field B_T=2.5 T, plasma current I_p=1.2 MA, line averaged density $\bar{n}_e = 6.3 \times 10^{19} m^{-3}$, safety factor q_{95}=3.3 and average triangularity δ=0.15. The radial shift of the plasma column was used to get a dense spatial grid of measurement points for T_e and SXR radiation. Measurements during many ELM cycles were overlayed by mapping onto the time difference to the start of the preceding ELM Δt_{ELM}.

In Fig. 4 radial profiles of T_e, n_e and SXR radiation flux I_{sxr} are shown versus the radial distance of the flux surface to the separatrix at mid plane Δx. T_e (4a) and I_{sxr} are measured with high time resolution and are shown for a time point shortly after the ELM at Δt_{ELM}=1ms and shortly before the next ELM at Δt_{ELM}=9.5ms. The measurement of n_e is ELM averaged (4b). The SXR profiles are shown for two nearly identical discharges. Discharge #12970 was shortly after a siliconization of the vessel walls and 100µm thick Be-filters were used, such that I_{sxr} is strongly dominated by radiation from Si (4c,e). In #13158 a constant Ne puff was applied and 12µm thick Be-filters were employed. Here, the line radiation of Ne is dominant (4d,f).

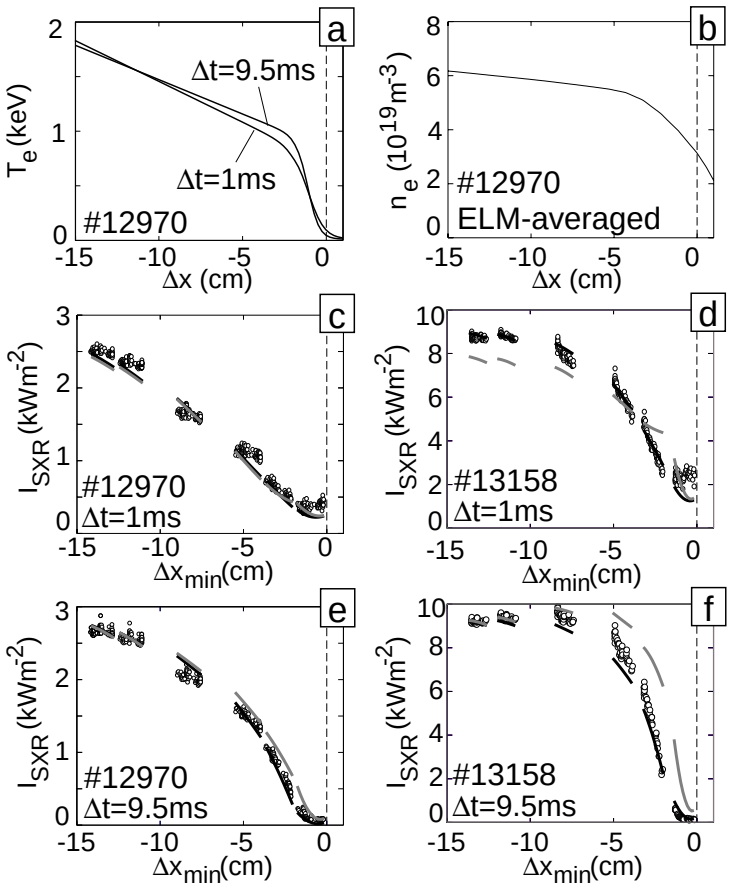

FIG. 4: T_e, n_e and SXR radiation flux I_{sxr} versus the radial distance Δx of the flux surface to the separatrix at mid plane at different times during an ELM cycle. The black (model **D***) and grey lines (model* **C***) in Fig. (c-f) are calculated SXR radiation fluxes assuming the two transport models from Fig. 5.*

The SXR signals are shown versus Δx_{min}, i.e. the radial coordinate of the flux surface, which is tangential to the lines-of-sight at the measurement time. For both impurities, a strong modulation of I_{sxr} during an ELM cycle is observed for $\Delta x_{min} \geq -10$cm, which can not be explained by the change of T_e or n_e. This is obvious for the channels which are nearly tangent to the separatrix (compare 4c with 4e and 4d with 4f for $\Delta x_{min} \approx 0$). Here, each ELM produces a large positive spike in a plasma region with $T_e \approx 100$eV.

The temporal evolution of I_{sxr} in both discharges was used to test the relevance of two 1D models for the edge impurity transport during an ELM cycle. The features of the two models are shown in Fig. 5. The generally accepted fact that each ELM leads to a loss of impurities in the confined region was the starting point of the two models. In model **D**, the ELM was assumed to cause a strong rise of the diffusion coefficient in the edge region without an outwardly directed drift velocity. Thus, the ELM can only cause a loss of the impurity content if the impurity density in the edge of the confined region develops a negative slope in the quiet phase of an ELM cycle. Since the impurity source is located outside the separatrix, an inwardly directed pinch must be present in the quiet phase. In model **C**, the ELM induces a reduced rise of the diffusion coefficient and a strong outwardly directed drift velocity to cause a loss of impurity content. Here, the transport in the quiet phase is purely diffusive. The diffusion coefficient in the quiet phase was set equal in both models. D strongly decreases from the edge to the center for $\rho < 0.85$. A maximum value of D_{max}=2m^2/s was used. In the region of the edge transport barrier the diffusion coefficient was set to D_{edge}=0.5m^2/s. The values of D_{max} and D_{edge} are consistent with measurements

of the impurity decay times after Si-LBO in this type of discharges, however, a lower value of D_{edge} would be equally consistent, if the location of the transport barrier is moved towards the separatrix. The loss of impurity content during an ELM is ≈6% in both cases.

The impurity density distribution and the according SXR radiation during an ELM cycle were calculated with STRAHL for both models. The background SXR emission due to carbon was considered using the concentration from charge exchange recombination spectroscopy (CXRS) with values of $c_C \approx 1\%$. For the discharge with Ne-Puff (#13158), 0.04% Si concentration was assumed in accordance with the emission before the start of the Ne-puff. The calculated SXR emission was integrated along the lines-of-sight and the evolution of the calculated radiation fluxes is compared with the measurements in Fig. 4. The black lines in Fig. 4c-f give the results for model **D** while the grey lines show the radiation fluxes for model **C**. In #12970, model **D** gives a better agreement for the profile before the ELM (4e). The results from model **C** would agree with the same profile (4e) when turning the poloidal angle of the SXR camera by 0.5^o, which is within the present uncertainty of the measured camera orientation. The profile after the ELM (Fig. 4c) is equally well described by the models and the agreement gets worse when turning the camera orientation. For #13158 (Fig.4d,f), the differences of the two models can be seen more clearly, since He- and H-like Ne radiate at lower temperatures. Again, model **D** gives a better agreement after (Fig. 4d) and before the ELM (Fig. 4f). A mix of **C** and **D** with outward drift during the ELM and inward drift inbetween ELMs showed good agreement before the ELM and a poor fit after the ELM. Thus, an edge transport model with an inward pinch inbetween ELMs and diffusive transport during the ELM yields the best description of the measurements. Further improvement of this analysis by inclusion of ELM-resolved n_e measurements is envisaged. Transport model **D** is also supported by CXRS-measurements of the C^{6+}-density. The ELM-averaged density profiles of C^{6+} can only be explained when assuming an inward pinch at the plasma edge.

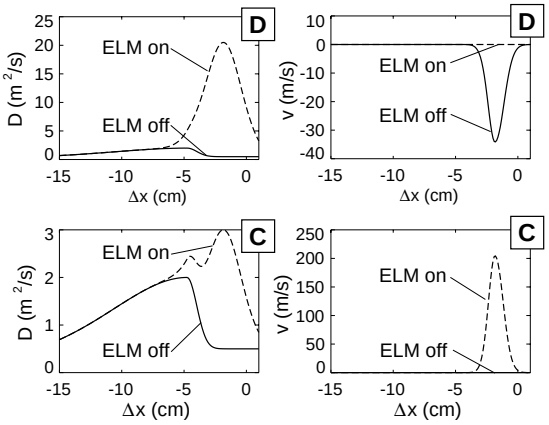

FIG. 5: Two models for D and v *at the plasma edge during an ELM and in between ELMs versus the radial distance of the flux surface to the separatrix at midplane* Δx.

References

[1] GIANNELLA, R. et al., Nucl. Fusion **34** (1994) 1185.
[2] DUX, R. et al., Nucl. Fusion **39** (1999) 1509.
[3] SUMMERS, H. P., JET-IR 06 (Abingdon: JET Joint Undertaking) (1994).
[4] BEHRINGER, K., JET-R(87)08, JET Joint Undertaking, Culham (1987).
[5] DUX, R. and PEETERS, A. G., Nucl. Fusion **40** (2000) 1721.
[6] HIRSHMAN, S. P. and SIGMAR, D. J., Nucl. Fusion **21** (1981) 1079.
[7] HOULBERG, W. A. et al., Phys. Plasmas **4** (1997) 3230.
[8] PEETERS, A. G., Phys. Plasmas **7** (2000) 268.